Influence of electronic vs nuclear energy loss in radiation damage of Ti_3SiC_2

William A. Hanson[a,*], Maulik K.Patel[a,b], Miguel L. Crespillo[a], Yanwen Zhang[a,c], William J. Weber[a,c,*]

[a]*Department of Materials Science & Engineering, The University of Tennessee, Knoxville, TN, 37996, USA*
[b]*Department of Mechanical, Materials & Areospace Engineering, University of Liverpool, L69 3GH, UK*
[c]*Materials Science & Technology Division, Oak Ridge National Laboratory, Oak Ridge, TN, 37831, USA*

Abstract

The thermal conductivity and stability of MAX phases has led to irradiation studies of these materials for their possible application in the hostile environments of high temperature and radiation. Numerous neutron and ion irradiation studies have been conducted that demonstrate that radiation induced modifications consists of lattice strain and increased formation of TiC. Ion beams have been used to simulate damage created by neutrons; however, what is not clear is the effect of varying electronic to nuclear energy loss on the damage evolution within this material. In the present work, changes in c/a within Ti_3SiC_2 are monitored as a function of energy deposition at constant damage dose following high fluence 9 *MeV* Ti ion irradiations at room temperature. The results reveal that there is an apparent threshold in the electronic energy loss, above which the c/a ratio and TiC concentration starts to increase with increasing electronic energy loss. Interestingly, this change is independent of the damage dose in displacements per atom. This suggests that inelastic energy dissipation is of paramount importance when selecting ions for simulating damage by energetic neutrons.

Keywords: Ion irradiation, Ti_3SiC_2, X-ray diffraction (XRD), TEM, Electronic stopping

1. Introduction

$M_{n+1}AX_n$ (MAX) phases are being debated as a candidate structural material, such as cladding or core materials, for future generation fission and fusion reactors. These phases are a class of ternary carbides and nitrides, where M is an early transition metal, A is an A group element, and X is either C or N. They crystallize in a hexagonal structure within the $P6_3/mmc$ space group composed of n-M_2X rhombohedra separated by A-element basal monolayers, see supplementary figure (S.Fig. **1**). This nanolamellar crystalline structure results in a unique combination of thermophysical properties that make them potentially interesting for applications in demanding environments like those existing in aerospace and advanced fossil and nuclear energy applications [1–6]. Several compositions, including Ti_3SiC_2, Ti_3AlC_2, and Ti_2AlC, have been the subject of many irradiation studies, using neutrons and ions, [7–16] due to their high thermal conductivity, thermomechanical and phase stability, [5, 6, 17], resistance to thermal shock [6], corrosion resistance [18], and low neutron absorption cross section that is comparable to SiC [19].

In general, irradiation damage in MAX phases typically leads to an increase in TiC concentration and lattice strain, specifically an increase in the c/a lattice parameters (c,a-LPs), and this is no different for Ti_3SiC_2, the subject of this study [9, 11–13, 15, 16, 20, 21]. TiC can form in pristine MAX during synthesis due to a stoichiometric mismatch [6, 13] and shares many structural similarities with the MAX structure. In fact, if the A-layer of Ti_3SiC_2 MAX phase is ignored, the resulting structure is identical to a nano-twinned TiC [6]. This TiC is more brittle and less thermally conductive than the MAX phase. Further, it has been suggested that the nano-layered structure, specifically the presence of the A-layer, is a primary source for irradiation damage resistance for the MAX phase [13, 14, 20, 22], acting as a sink for point defects and a high diffusivity path for recombination [14, 16, 23]. Thus, the presence of TiC in MAX

*Corresponding authors:
(W.A. Hanson) *email:* walexhanson@gmail.com; whanson@vols.utk.edu; *Tel.:* +1 2406785745
(W.J. Weber) *email:* wjweber@utk.edu; *Tel.:* +1 8659740415

phase bulk can partially offset the beneficial properties of the layered structure for their application in extreme environments [3, 4]. Although there is a lack of agreement in the mechanisms responsible for TiC concentration increases [8, 10, 24], we propose that the changes of TiC can still represent a qualitative metric for irradiation damage within Ti_3SiC_2 and other Ti containing MAX phases. There is, however, difficulty in quantifying this change in concentration following irradiation due to the similarities between the MAX phase and TiC structures and their resulting diffraction profiles.

It is well understood that ion irradiations may be used to mimic the radiation damage processes and microstructural features observed in materials subjected to neutron irradiation environments. Ion irradiations have the further advantage of being able to systematically explore specific aspects of irradiation conditions and reach very high damage doses in displacements per atom (dpa) with little to no resulting radioactivity in samples. However, high energy ion beams result in inelastic collisions with electrons, or electronic stopping, resulting in intense ionization until the ion energy is reduced sufficiently for elastic collisions with atomic nuclei, or nuclear stopping, and damage cascades to dominate [25, 26]. Therefore, knowing the response of a material to these electron ionization events is of paramount importance when selecting ions as a complimentary tool for comparison with neutron irradiation results.

It has been previously demonstrated that Ti_3SiC_2 irradiated by ions with energy in the electronic stopping regime remain crystalline under most irradiation conditions. This includes thin film, *in situ* irradiations up to 25 dpa [8] and low temperature irradiations. Though a high degree of crystalline disorder may result, the MAX phase structure remains relatively intact and does not fully amorphize [14]. It has been suggested that a low Ti_{Si} antisite formation energy for Ti adjacent to the Si layer may contribute to the amorphization resistance by occupying V_{Si} sites [23]. However, a lack of amorphization is not the same as an insensitivity to electronic excitation and ionization effects.

Strain in the c-LP with little to no corresponding volume change was observed following 92 MeV Xe irradiations [7], and a similar response followed 74 MeV Kr irradiations [9]. In both these cases, the structural changes were observed in depth regions dominated by electronic stopping. These results were subsequently compared to low fluence irradiations with 930 MeV Xe ions, and little structural change and no black spot defects were observed as compared to regions dominated by elastic collisions [7, 9]. Based on these results, Ti_3SiC_2 was deemed insensitive to electronic excitations, and the observed results were attributed to elastic collisions with atomic nuclei [9].

It should be noted, though, the swift heavy ion irradiations were conducted to a lower fluence and thus a significantly lower equivalent damage dose (dpa) and integrated electronic energy loss due to experimental constraints to prevent undesired *in situ* sample heating [9]. It is known that in other material systems, a minimum dose is necessary before electronic excitation results in structural change, and in materials sensitive to electronic interactions, increasing S_e typically reduces this incubation fluence [27–30]. Therefore, in an attempt to deconvolute the influences of elastic and inelastic collisions on resulting damage observed following ion irradiations, Ti_3SiC_2 was subjected to high energy, high fluence Ti self-ion irradiations. Fluences were selected such that precise measurement of lattice strain as a function of depth, utilizing a novel method, as well as changes in TiC profiles, allow for comparison of resulting damage at different energy depositions with comparable damage dose (dpa).

2. Experimental

2.1. Sample Preparations

The polycrystalline Ti_3SiC_2 used in this study was synthesized in bulk by the MAX phase research group at Drexel University via hotpressing; complete details for processing have been discussed previously and will not be discussed here [3, 31]. Four plate sections were cut via low speed diamond saw to $10 \times 10 \times 1$ mm and low stress polished with diamond lapping film and finishing with 0.05 μm colloidal silica.

Grazing incidence x-ray diffraction (GIXRD) profiles were gathered at the Joint Institute for Advanced Materials (JIAM) Diffraction Facility using a PANalytical X'Pert^3 MRD in grazing geometry equipped with a Cu x-ray tube, Si parabolic mirror, 0.04 *Rad* soller slits, $1/8^\circ$ divergence slit, and a 0.27° parallel plate collimator. The scans were performed at increasing incidence angles in all samples to probe depths from 0.5 μm – 2.0 μm in 0.25 μm intervals providing a depth profile of the pristine and irradiated conditions.

Three polished plates were then sectioned to 8×5 mm for irradiation and removed sections were preserved as pristine reference conditions. TEM lamella were prepared using a ZEISS Auriga scanning electron microscope (SEM) equipped with Ga focused ion beam (FIB) in the JIAM Electron Microscopy Facility. Lamella were lifted using low

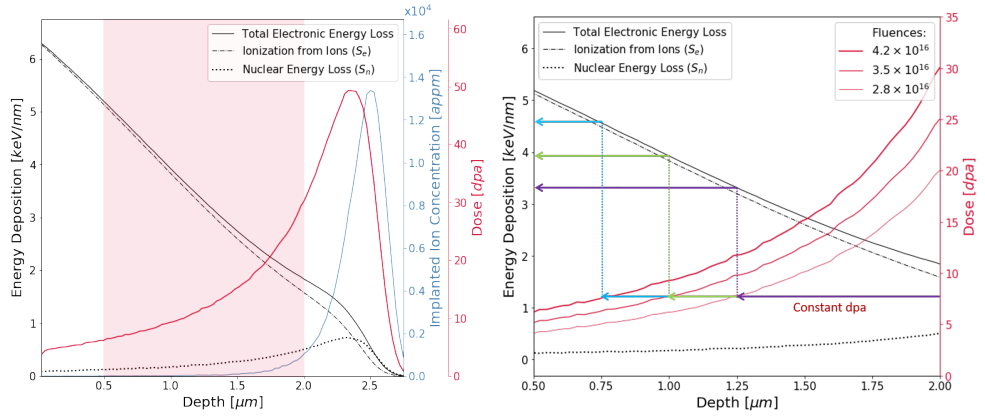

(a) (b)

Fig. 1 – (a) Energy deposition, damage dose (dpa), and Ti concentration as a function of depth for an ion fluence of $4.2{\times}10^{16}$ cm^{-2}. (b) Energy deposition and damage dose (dpa) for the three fluences in the present study. The depth region of interest (0.5-2.0 μm) is displayed by a red shaded region in (a), and shown in (b) are three depths probed, which correspond to the same damage dose but different electronic energy loss.

milling currents with Pt deposited on the surface to minimize artifacts from the sample preparation. FIB lamella preparations were conducted on both pristine and irradiated samples. TEM was performed using a ZEISS Libra 200 HT FE MC at an accelerating voltage of 200 kV, within JIAM, to obtain micrographs and gather selected area electron diffraction (SAED) patterns to analyze structural changes at deeper regions without surface contributions.

2.2. Ion Irradiation Conditions

Ion irradiations were conducted at The University of Tennessee Ion Beam Materials Laboratory (IBML) [32]. *Ab initio* molecular dynamics (AIMD) simulations have suggested that Ti is the easiest element to displace from its site, but it is likely to recombine with its own vacancy [33]. These simulations and initial SRIM (2013) [34, 35] calculations resulted in the selection of 9 MeV Ti^{3+} self-ions for the irradiation to provide the largest variation in electronic energy loss, as a function of depth. The full cascade SRIM (v2013) [34, 35] simulations of 9 MeV Ti in Ti_3SiC_2 were performed, and the resulting electronic and nuclear energy deposition, damage dose (dpa), and ion concentration profiles as a function depth are shown in Fig. **1a** for a fluence of $4.2{\times}10^{16}$ cm^{-2}, the maximum fluence selected for this study. These calculations utilized weighted average threshold displacement energies of 27.9, 30.6, and 25.7 eV for C, Si and Ti, respectively, as determined by previous AIMD simulations [33] and a theoretical density of 4.528 g/cm^3 as pristine lattice parameters match those in literature [6]. The ion energy places the resulting damage peak near the 2.0 μm maximum depth region of interest for this study, indicated by the shaded red box in Fig. **1a**. The selected ion fluences for this study are (2.8, 3.5, and 4.2)$\times10^{16}$ cm^{-2}, which correspond to a maximum damage dose of 20, 25, and 30 dpa, respectively, at the maximum depth region of interest (2.0 μm). The depth region of interest also avoids the Ti-ion concentration peak at ~2.5 μm, which is $1.3{\times}10^4$ $appm$ (1.34%) for a fluence of $4.2{\times}10^{16}$ cm^{-2}, see Fig. **1a**. Note that over the depth of interest, the Ti-ion concentration change is <35 $appm$ at a depth of 1.25 μm, and this only increases to ~1000 $appm$ by 2 μm, so the implanted Ti-ions should have little to no structural or chemical influence. The sample surface was oriented normal to the beam and ion flux was kept below $2{\times}10^{12}$ $cm^{-1}s^{-1}$ to reduce any undesirable sample heating and charge accumulation for room temperature (RT) irradiations [36].

In addition to the 9 MeV Ti ions resulting in a variation in local damage dose as a function of depth, the fluences selected provide the opportunity to explore changes in energy deposition at comparable damage doses, see Fig. **1b** for an example. In this case, it can be seen that by probing different depths for these ion fluences, three different energy depositions may be compared at the same damage dose, effectively isolating the effects of electronic stopping from damage dose. In total, electronic energy loss varies from approximately 5.20 – 1.83 keV/nm over the ranges probed of 0.5 – 2.0 μm, respectively.

2.3. Iterative Self-consistent c/a Method

GIXRD was utilized to analyze structural changes as a function of depth from 0.5-2.0 μm at 0.25 μm intervals with a step size of 0.02° 2θ . Grazing angles were calculated using the X-ray Interactions with Matter data tables developed by The Center for X-ray Optics [37]. While TiC is a slightly better x-ray attenuator than Ti_3SiC_2, x-ray penetration behavior as a function of grazing angle is proportionate between the two materials. A linear relationship exists between phase concentration and the corresponding x-ray attenuation; therefore, care was taken to estimate TiC concentrations from relative peak intensities such that appropriate grazing angles were selected for the desired depths. That said, it is conventional to use consistent grazing angles between compared samples, so with anticipated variation in TiC concentrations between irradiation conditions, an upper bound of 20% error was assumed in these concentration estimations. However, given the similarity in x-ray attenuation between Ti_3SiC_2 and TiC, this only results in an average maximum calculated depth error of 0.04 μm for the selected grazing angles, so the depths probed between samples were consistent.

Scans from 7-82° 2θ were gathered with a count time of 3 $s/step$ and longer scans over shorter ranges of 33-45°, 57-64°, and 70-80° 2θ were gathered with count times of 6, 7, and 8 $s/step$, respectively, to allow for better counting statistics in critical regions where peak shifts were expected. However, accurate changes in lattice parameters between pristine and ion-irradiated conditions cannot be directly determined from peak position shift within hexagonal systems alone because the ratio between the c-LP and a-LP (c/a) must first be known [38].

It should be noted that there are many ways to arrive at this ratio. It may be determined by performing Rietveld refinements [39]; however, most software developed for this method do not fully account for x-ray absorption due to the grazing angle [40]. Additionally, it has been demonstrated that damage within the structure further complicates performing detailed analysis using this method [11]. Given that GIXRD is vital to this study and structural damage in some form is expected following ion irradiation, Rietveld analysis is not utilized in this study. It is also possible to select a c/a ratio from literature sources. That said, given previous ion irradiation results in this system, which demonstrate lattice distortion [9, 11, 13, 15, 20], it is unrealistic to assume the c/a ratio remains undistorted, thus making literature c/a ratios not viable for this application. Furthermore, c/a can be directly calculated by selecting peaks that isolate contributions to the c and a-LPs eg: the (008) or (110), respectively. The issue with this method is that it severely limits the number of peaks that can contribute to the calculation.

Finally, the method utilized in this study is to use all the peaks measured to iteratively determine a c/a value that is self-consistent. The GIXRD profiles were corrected for Lorentz-polarization and absorption effects on intensity, as these can influence the peak position [38]. The resulting corrected profiles were indexed, and the peaks were fit using Origin-Pro [41].

The first step in the iterative method is to assume a c/a value from the literature and use the indexed peak locations in the relationship:

$$\langle a(\phi,\psi)\rangle_{(hkl)} = \langle d(\phi,\psi)\rangle_{(hkl)} \cdot \cdot \left\{\left[\frac{4}{3}\cdot\left(h^2+hk+k^2\right)\right] + \frac{l^2}{(c/a)^2}\right\}^{\frac{1}{2}} \tag{1}$$

$$\psi_{(hkl)} = \theta_{(hkl)} - \omega \tag{2}$$

where a is the calculated a-LP, d is the measured d-spacing for each peak, and ψ is determined using Eq. **2** by peak location and incident grazing angle, ω. The rotational orientation of the sample relative to the diffraction plane defines *phi*, and multiple measurements at different *phi* may be performed if this method is used to determine an applied stress tensor relative to the laboratory basis. However, this is not necessary for using the iterative method to determine a self-consistent c/a, as texture has been demonstrated to not affect the c or a-LPs determined by this method. Therefore, in this case, phi is arbitrary and may be treated as zero, so long as all grazing ω are gathered consistently from the same rotational orientation for each sample [38, 42, 43]. It should be noted that this method is stable, and the quality of the assumed c/a value from the literature only determines the number of iterations needed for the c/a to converge on a self-consistent value, and even an 80% error in the initial assumed c/a does not influence the converged c/a value. Once the a-LPs are calculated for each peak using Eq. **1**, they are used to find the values for the stress (σ_{ij}) and initial a-LP (a_0) via least squares fit of the relationship [38]:

$$\langle a(\phi,\psi)\rangle_{(hkl)} = \left[F_{ij}(hkl,\phi,\psi)\cdot\sigma_{ij}\right]a_0 + a_0 \tag{3}$$

where $F_{ij}(hkl,\phi,\psi)$ are the X-ray Elastic Constants (XECs) determined previously based on sample orientation as detailed by Victor Hauk and Baczmanski *et al.* [44, 45] using known elastic properites for Ti_3SiC_2 [5]. Once σ_{ij} and a_0 are known, Eq. **3** is used again in reverse to determine theoretical values for the a-LP for each peak, once again based off the already determined XECs. These calculated a-LP values are used with the experimentally determined d-spacings in Eq. **4** as defined by the relations in Eq. **5** [38].

$$y = px\ ,\ where: \tag{4}$$

$$\begin{aligned} p &= \frac{1}{(c/a)^2} \qquad\qquad x = l^2 \\ y &= \left[\frac{\langle a(\phi,\psi)\rangle_{(hkl),\,calc}}{\langle d(\phi,\psi)\rangle_{(hkl),\,exp}}\right]^2 - \left[\frac{4}{3}\cdot(h^2+hk+k^2)\right] \end{aligned} \tag{5}$$

A linear fit is performed on Eq. **4** to find the slope and thus a calculated c/a ratio as defined in Eq. **5**. This new c/a is then inserted in Eq. **1** in place of the assumed c/a from the first cycle, and the processes is repeated iteratively until c/a has converged at a single value. Then Eq. **1** may be used one a last time to determine the c and a-LPs for each peak that contributed to the self consistent c/a, using its experimentally measured d-spacing. This technique not only determines a more accurate c/a value than what may be estimated given the expected lattice distortions, it utilizes all fit peaks to determine c/a, thus returning a value that is self-consistent within the profile [38]. Further, each fit peak then also contributes to the final determined lattice parameters, so the average c and a-LPs for each grazing profile are reported along with the standard deviation of the values. To the best of our knowledge this is the first time this method has been applied to determine structural changes in lattice parameter within ion-irradiated hexagonal materials.

3. Results

3.1. Grazing Incidence X-ray Diffraction

3.1.1. Disorder and Peak Shift

GIXRD profiles about the (110) peak of Ti_3SiC_2 for three different fluences and the pristine condition are shown in Fig. **2**, with relative intensity normalized and staggered; in addition, the intensity is also plotted as a heat map in the background. Each profile was collected from a different depth such that an equivalent damage dose of 7.6 dpa is probed for each fluence while electronic stopping is varied, as demonstrated in Fig. **1b**. Since the pristine profiles for each depth are equivalent in peak position, the deepest corresponding depth is also indicated. Initial observations clearly show an apparent increase in TiC at all depths with broad disordered peaks dominating the relative intensity of the profiles when probing shallower depths. The Ti_3SiC_2 phase is easily observed, contributing intensity at all depths, and appears to show little to no signs of broadening in the peaks, though it is difficult to judge peak broadening effects in the shallowest depths where TiC relative intensity dominates the profile. For additional examples, the full GIXRD profiles for the pristine and irradiated conditions at the boundaries of the depths of interest and an intermediate depth are provided in S.Fig. **2**. Peak shifting is also only evident in the shallower depths probed. This is especially clear when comparing depths probing comparable damage doses, as shown in Fig. **2**. For example, the three irradiated profiles shown in Fig. **2** probe different depths at the consistent damage dose of 7.6 dpa, and the (110) peak clearly shifts to higher *degrees* 2θ with decreasing depth probed. This indicates a contraction of the a-LP relative to pristine values at depths were electronic stopping dominates.

3.1.2. Lattice Parameter Analysis

Utilizing the iterative self-consistent c/a method, lattice parameters for each condition have been determined as a function of depth, as shown in Fig. **3a** and **3b**. The pristine profile shows consistent c and a-LPs without statistical change, and the irradiated samples have c and a-LP values comparable to pristine values at deeper regions, 1.25-2.0

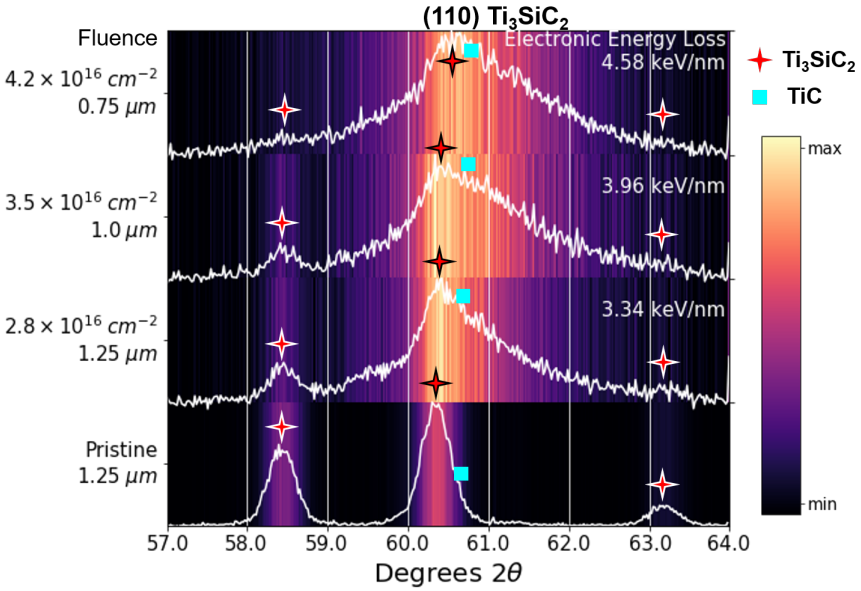

Fig. 2 – (110) peak profiles obtained from Ti_3SiC_2 irradiated at three different fluences. Each profile was collected from a different depth that corresponds to the same damage dose (7.6 dpa) but different electronic energy loss.

μm, where the damage dose is higher. As indicated by the (110) peak shifting in Fig. **2**, all observed lattice strain is isolated to the shallower regions, where the damage dose is lower and electronic stopping is dominant. At a fluence of $2.8{\times}10^{16}$ cm^{-2}, contraction of the c-LP and expansion of the a-LP are evident while for a fluence of $4.2{\times}10^{16}$ cm^{-2}, the opposite behavior, with c-LP expansion and a-LP contraction, is apparent. This latter result is similar to results observed previously in literature under predominantly ballistic damage conditions, and the scale (~0.2% for a-LP contraction and ~0.3% for c-LP expansion) is comparable as well [11, 13, 15, 16, 20]. At the intermediate fluence of $3.5{\times}10^{16}$ cm^{-2}, only minor contraction of the a-LP and expansion of the c-LP are observed.

By applying the similar groupings of damage dose at different depths, it is possible to compare lattice strain in the system as a function of the energy deposition, as shown in Fig. **3c** and **3d**. At this point, a trend is clearly visible that in each grouped case, increases in electronic energy loss correlate to relative expansion in the c-LP and contraction in the a-LP. Further these trends only appear to begin at electronic energy loss levels higher than a threshold level of 4 keV/nm. Reexamining the peak shifting at 7.6 dpa in Fig. **2**, the shifting of the (110) peak is clear at depths where electronic energy loss exceeds 4 keV/nm, and TiC dominance in the profile increases with increasing electronic energy loss.

3.2. TEM

The TEM lamella were oriented on the $[2\bar{2}01]$ zone axis and SAED patterns were gathered with the selected area aperture exposing approximately 0.25 μm diameter section of the sample, as illustrated in Fig. **4a** and **4b**. The $[2\bar{2}01]$ zone axis was selected because the MAX structure has near extinctions at this orientation for the $\{0\bar{1}1\bar{2}\}$ reflections; meanwhile nano-twinned TiC has significant intensity contribution for these reflections in the same orientation. Looking at the depth profiles from the irradiated surface of both the most and least exposed samples ($4.2{\times}10^{16}$ and $2.8{\times}10^{16}$ cm^{-2}, respectively), it is clear that the material is highly crystalline with only slight ring intensity, likely an artifact from FIB lamella preparation in this region; full depth profiles are included in S.Fig. **3** and **4**. It is also important to note that in all cases there is large intensity from what is believed to be nano-twinned TiC structure in the regions closer to the irradiated surface; while at the deeper irradiation regions from 1.25 to 2.0 μm, the intensity returns to near extinction levels typical of the Ti_3SiC_2 structure. The $4.2{\times}10^{16}$ cm^{-2} sample shows some intensity at the greater irradiation depths, but this is significantly weaker than that observed in shallower regions. This appears to corroborate what was observed previously in the GIXRD results where Ti_3SiC_2 peaks were strong at deeper depths

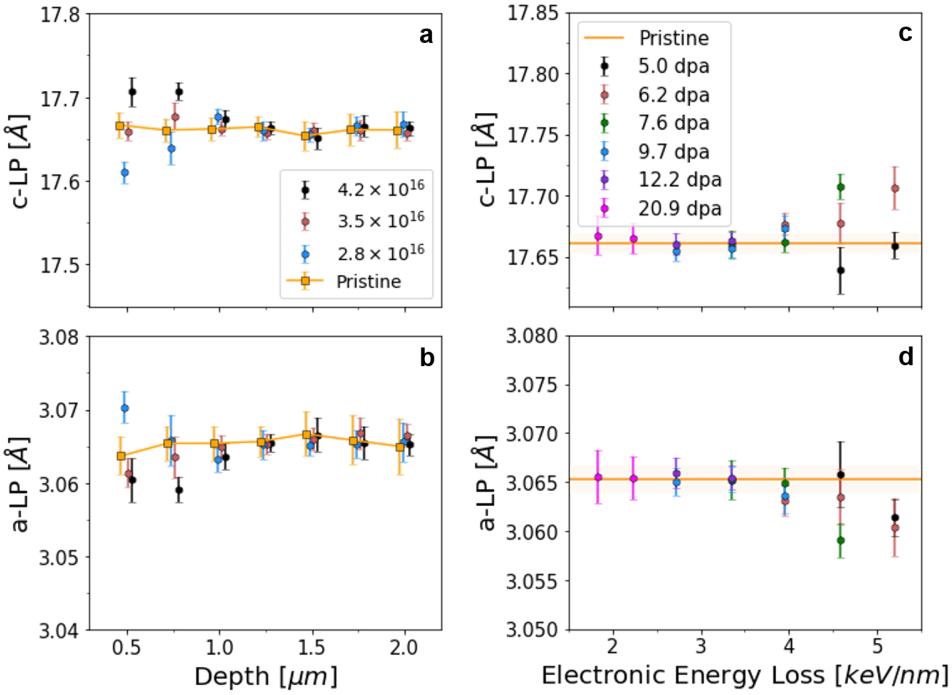

Fig. 3 – Lattice parameters (LPs) calculated as a function of depth in (a) and (b) and as a function of electronic energy loss in (c) and (d).

probed, while broad TiC peaks were still visible (recall that grazing incidence techniques include a signal from regions shallower than the desired depth; though, this signal is weaker). These SAED depth profiles, which are isolated from irradiation surface conditions, further suggest that structural changes occurred in regions near the irradiation surface, where electronic stopping dominates, rather than where predicted damage dose is greater. This is evident when observing that the nano-twinned TiC $\{0\bar{1}1\bar{2}\}$ reflections are only visible in Fig. **4a**, where electronic energy loss exceeds 4 *keV*/*nm*, while a near extinction of these reflections is present when below this threshold in Fig. **4b**, despite each region corresponding to an equivalent damage dose of 7.6 dpa.

4. Discussion

4.1. Structure Analysis

Past studies have also observed major broadening in GIXRD peak profiles apparently isolated to peaks attributed to TiC, while broadening of MAX peaks by comparison is observed to be less significant [10, 11]. A possible source for these isolated intensity changes can be seen by examining the structure factors of disordered Ti_3SiC_2 supercells, including defects, as proposed by Liu *et al.* [33]. Minor peak intensity is observed in the profiles of partially disordered supercells near where TiC is expected in the profile. Given the largely unbroadened nature of the MAX profiles observed, this could suggests that a partially disordered MAX structure may contribute to the broad observed intensity at these peak sites rather than a full decomposition of the MAX phase into TiC. It has been previously proposed that the Ti_3AlC_2 composition, which shares its structure with Ti_3SiC_2, may form a chemically disordered structure that exhibits peak profiles similar to TiC_x [46]. The potentially convoluted contribution to the broad intensity near the TiC peaks makes it difficult to quantify exactly the changes in concentration, but qualitatively it is clear that the relative intensity increases with decreasing depth and increasing electronic energy loss, as illustrated in Fig. **2**. This parallels what is observed in the SAED patterns in Fig. **4a** and **4b**, where features similar to nano-twinned TiC intensity are observed.

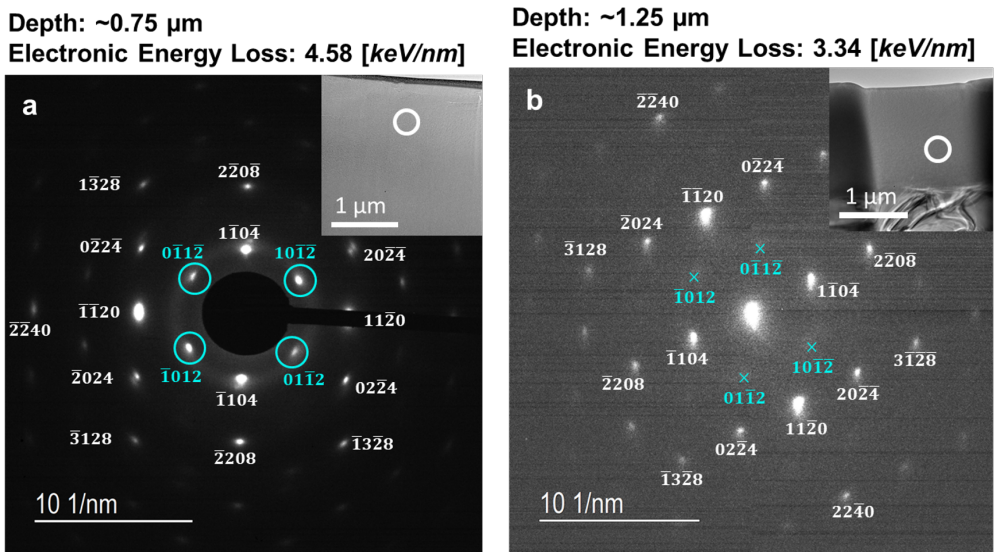

Fig. 4 – SAED patterns probing irradiation depths consistent with a damage dose of 7.6 dpa for the (a) $4.2{\times}10^{16}$ and (b) $2.8{\times}10^{16}$ cm^{-2} conditions. The insets demonstrate the SAED aperture positions from the irradiation surface to accomplish this and each sample is oriented about the $[2\bar{2}01]$ zone axis. Blue rings encircle intensity believed to be due to nano-twinned TiC in (a) while near extinction values typical of the Ti_3SiC_2 are indicated by blue × in (b).

The observed lattice strain results may be explained by interstitials trapped within the A-layers. Xiao *et al.* [47] proposed these interstitials reside in-plane on the hexagonal interstitial sites (I_{hex}), which are the most energetically favorable sites under equilibrium conditions. In contrast, AIMD simulations by Liu *et al.* [33] revealed that interstitials created by threshold displacement events often reside in-plane on the prismatic interstitial sites (I_{pri}); though, in many cases, Ti interstitial (Ti_I) also formed split interstitials with neighboring Ti atoms (Ti2 site) above the I_{hex} sites between planes. In either case, these proposed defect diffusion mechanisms and sites could account for the changes in lattice parameter observed in the shallowest regions in Fig. **3a** and **3b**.

It is important to note that the implanted Ti-ions may be discounted as a potential source for the observed relative strain for a couple reasons. First, their concentration profile is very low and changes little over much of the depths probed, reaching <10 $appm$ by 1.0 μm from the irradiation surface, see Fig. **1a**. This should be insufficient to account for the relative strain observed at these shallower depths. Second, even if this low concentration was sufficient to contribute to the strain observed, the strain should then be at its greatest when the depth probed is doubled to 2.0 μm, as the Ti-ion concentration is then increased by two orders of magnitude from ~10 to 1000 $appm$. However, c and a-LPs are comparable to pristine values at these greater depths, see Fig. **3a** and **3b**, so relative strain does not increase with depth and Ti-ion concentration.

It has been calculated recently that Ti_{Si} antisites should result in expansion and contraction of the c and a-LP, respectively, while C Frenkel pairs should lead to expansion of the a-LP and less expansion of the c-LP [16, 23, 47]. Given the similarity of their in-plane site occupancy, it is expected that Ti_I would have a similar influence on the c and a-LPs; though, in the case of the split Ti_Is, c-LP expansion and a-LP contraction is expected. While the barriers to migration for interstitials in and adjacent to the A-layer have been calculated to be relatively low, full occupancy of interstitial sites in the Ti_3C_2 layers effectively limit migration of point defects to 2-dimensions and further reduce the migration capabilities of Ti_{Si} antisites [16, 23, 47, 48]. Higher temperatures have been suggested as providing sufficient energy for point defect mobility beyond 2-dimensions for recombination [22, 48], but at room temperature, it appears the recombination is partially limited by this structural confinement of the defects. The results in Fig. **3a** and **3b**, could be explained by initially trapped C_I and Ti_I within the basal layers, which with increased ion fluence either saturate or migrate to sites adjacent to the basal layer, thus resulting in the apparent relaxation to pristine LP values at the intermediate fluence.

Given that TiC appears confined to the depths where this relative strain is observed, it is likely this structural confinement plays a role; though, until a thorough defect analysis is conducted, the precise role TiC plays remains unclear. It should also be acknowledged that it is possible that the seeming reverse in strain observed could be relaxation with increasing fluence from strain induced via polishing. However, given the consistent LPs recorded in the pristine sample at each depth in comparison to ion-irradiated samples when they were still pristine, this seem unlikely.

4.2. Electronic Stopping Implications

A clear correlation has been observed between the near surface LP strain behavior and the calculated electronic stopping values, as shown in Fig. **3c** and **3d**. At comparable doses, increasing electronic energy loss results in increased c-LP expansion and a-LP contraction above an apparent electronic stopping threshold of 4 keV/nm. The same can be said for apparent TiC concentration increases in the near surface regions above the same threshold, Fig. **4a** and **4b**. In the past, little defect production or lattice strain has been attributed to electronic stopping at levels below 28 keV/nm [9], but to our knowledge the influence of electronic energy loss has not been explicitly explored at fluences such as those employed in this study. Further, without the self-consistent c/a method utilized here, the strain effects may not have been readily visible within the lab scale testing environment.

While this observed strain, where electronic stopping dominates, might be attributed to an artifact of surface irradiation effects, this may be discounted for multiple reasons. Surface effects are typically exhibited as defect-free denuded zones adjacent to free surfaces and grain boundaries that are often limited to the first 100-200 nm of depth [26]. For this study, the shallowest depth probed is well beyond this typical depth of influence. Additionally, following high temperature neutron irradiation studies, defect-free denuded zones were only observed when irradiation temperatures exceeded $735°C$ [20, 22], which suggests higher temperatures are needed for irradiation assisted annealing of defects near free surfaces and grain boundaries. Therefore, there should not be much in the way of surface effects within Ti_3SiC_2 during RT, low-flux irradiations.

It is likely these electronic effects are not due solely to electronic energy loss of single ions within the MAX structure. The ionization energy from a single 9 MeV Ti ion transferred to the lattice via electron-phonon coupling results in a thermal spike of $\sim$1000 K in pristine MAX phase. This is likely insufficient to account for the observed defect production and eventual strain. It has been demonstrated that there is often a synergy between electronic energy loss and evolving defect concentrations, whereby evolving defects can significantly affect the dissipation of electronic energy loss, such that the thermal spike is more radially confined and greatly increased in temperature [28, 30, 49–53]. In a recent study by Xue *et al.* [50], SiC was found to have an electronic energy loss threshold of 1.0 keV/nm for in-cascade annealing, whereby a highly localized thermal spike serves to suppress defect accumulation and even heal pre-existing defects. Conversely, in zircon, this localized heating in the ion path has been shown to additively increase damage production, even when electronic energy loss is below 1.0 keV/nm [28]. It has also been shown in lithium niobate [33] and in strontium titanate, when electronic energy loss exceeding 7.0 keV/nm [30], that the nuclear and electronic stopping interact synergistically as pre-existing defects inhibit electrical and thermal conductivity, which likely increases the influence of the thermal spike. Resultant damage track formation then increases in diameter with proportional increases in either electronic stopping or defect concentrations.

The results in the present study may parallel the behavior in zircon, lithium niobate, or strontium titanate as exceeding an electronic energy loss threshold of 4.0 keV/nm results in increases in the c/a ratio and diffraction intensity resembling nano-twinned TiC in the SAED patterns. This seems to suggest that above this threshold, electronic energy loss contributes to defect production and lattice strain. It has been demonstrated in the past that following low-dose neutron irradiations, there is a significant reduction in the conductivity of the Ti_3SiC_2 [13]. It is possible the elastic component, in this study, results in a similar effect to that observed in strontium titantate, whereby the thermal spike is enhanced and above 4.0 keV/nm, damage is observed. However, it may be the case that electronic ionization directly affects the material response, regardless of elastic contribution, as in the case of zircon, so drawing a conclusion as to the mechanism at this stage would be highly speculative.

That said, while a precise mechanism remains ellusive at this point, it is clear electronic energy loss plays a key role in the observed effects, and it is important to emphasize the apparent independence of the observed threshold from damage dose. Below the 4 keV/nm threshold, damage doses as high as 30 dpa in the 4.2×10^{16} cm^{-2} sample show no signs of strain relative to pristine values and have no signature from nano-twinned TiC visible in the SAED patterns. Meanwhile, the opposite occurs at lower damage dose levels in regions where electronic energy loss exceeds

the 4 keV/nm threshold. These results confirm that these structural changes are influenced by electronic energy loss rather than changes in damage dose. It is further important to note that this is a true energy threshold to structural change. While nuclear stopping is significantly higher at depths below the 4 keV/nm threshold, as can be seen in Fig. **1a**, it is clearly demonstrated that the majority of energy dissipation is still due to electronic stopping effects. Yet being below the threshold, the structural changes are not observed. There are also implications for future comparison between neutron and ion irradiation results. Electronic energy loss must be taken into consideration when selecting ions for studying irradiation damage events within this material. Once the effects observed in these preliminary results have been more thoroughly investigated, defect analysis will be necessary to more fully understand the implications of these results. Further, the influence of temperature will be explored in future irradiation studies to evaluate the effects of electronic energy loss under different conditions as well as an independent separate effects study to isolate the elastic and inelastic influences.

5. Conclusions

Structural changes due to irradiation with 9 $MeV\ Ti^{3+}$ ions at room temperature have been characterized to be confined to near surface regions where electronic stopping dominates. These structural changes are believed to be associated with features similar to nano-twinned TiC, as well as strain in both the c and a-LPs of the Ti_3SiC_2 structure. A self-consistent c/a method was applied in this study to measure the fine changes in the c and a-LPs as a function of grazing angle. To our knowledge, this is the first time this method has been applied to study the structural effects of ion-irradiation and modification of hexagonal systems. Consolidation of results within comparable damage doses (dpa) further revealed trends that the TiC signal and increase in c/a ratio through lattice strain are correlated to increasing electronic energy loss above a threshold of 4 keV/nm. Below this threshold, no nano-twinned TiC signal is observed in the SAED patterns, and c and a-LPs measured through the iterative method are comparable to pristine values, even at a damage dose of 30 dpa. It is still unclear as to the precise mechanisms that lead the observed effects of electronic energy loss, whether a direct effect or synergistic interaction with evolving damage; however, it is clear that electronic energy loss behavior of ions is of vital importance when selecting ions as a complimentary tool to neutron irradiations.

6. Acknowledgments

This research was supported by the University of Tennessee Office of the Chancellor and the University of Tennessee Governor's Chair program. The authors would like to thank Dr. John Dunlap and Dr. Gerd Duscher for their assistance and advice in performing SEM/FIB and TEM within the Joint Institute for Advance Materials Microscopy Facility. The authors would also like to thank Dr. Michael Koehler for his assistance within the Joint Institute for Advanced Materials Diffraction Facility. Finally, the authors would like to thank Chris Ostrouchov for his invaluable assistance with Python 3.6 programming to implement the iterative c/a method.

7. References

[1] V. H. Nowotny, Strukturchemie einiger Verbindungen der Übergangsmetalle mit den elementen C, Si, Ge, Sn, Progress in Solid State Chemistry 5 (C) (1971) 27–70. doi:10.1016/0079-6786(71)90016-1.

[2] H. Nowotny, P. Rogl, J. C. Schuster, Structural chemistry of complex carbides and related compounds, Journal of Solid State Chemistry 44 (1) (1982) 126–133. doi:10.1016/0022-4596(82)90409-1.

[3] M. W. Barsoum, T. El-Raghy, Synthesis and characterization of a remarkable ceramic: Ti3SiC2, Journal of the American Ceramic Society 79 (7) (1996) 1953–1956. doi:10.1111/j.1151-2916.1996.tb08018.x.

[4] M. W. Barsoum, The Mn+1AXn Phases: A new Class of Solids; Thermodynamically Stable Nanolaminates, Prog. Solid St. Chem. 28 (2000) 201–281.

[5] T. H. Scabarozi, S. Amini, O. Leaffer, A. Ganguly, S. Gupta, W. Tambussi, S. Clipper, J. E. Spanier, M. W. Barsoum, J. D. Hettinger, S. E. Lofland, Thermal expansion of select Mn+1AXn(M=early transition metal, A=A group element, X=C or N) phases measured by high temperature x-ray diffraction and dilatometry, Journal of Applied Physics 105 (1) (2009) 1–8. doi:10.1063/1.3021465.

[6] M. Barsoum, MAX Phases: Properties of Machinable Ternary Carbides and Nitrides, Wiley-VCH, Weinheim, Germany, 2013.

[7] J. Nappé, P. Grosseau, F. Audubert, B. Guilhot, M. Beauvy, M. Benabdesselam, I. Monnet, Damages induced by heavy ions in titanium silicon carbide: Effects of nuclear and electronic interactions at room temperature, Journal of Nuclear Materials 385 (2) (2009) 304–307. doi:10.1016/j.jnucmat.2008.12.018.

[8] K. Whittle, M. Blackford, R. Aughterson, S. Moricca, G. Lumpkin, D. Riley, N. Zaluzec, Radiation tolerance of Mn+1AXn phases, Ti3AlC2 and Ti3SiC2, Acta Materialia 58 (13) (2010) 4362–4368. doi:10.1016/j.actamat.2010.04.029.

[9] J. C. Nappé, I. Monnet, P. Grosseau, F. Audubert, B. Guilhot, M. Beauvy, M. Benabdesselam, L. Thomé, Structural changes induced by heavy ion irradiation in titanium silicon carbide, Journal of Nuclear Materials 409 (1) (2011) 53–61. doi:10.1016/j.jnucmat.2010.12.235.
[10] C. Liu, L. Shi, Q. Qi, D. J. O'Connor, B. V. King, E. H. Kisi, X. B. Qing, B. Y. Wang, Surface damage of Ti3SiC2 by MeV iodine bombardment, Nuclear Instruments and Methods in Physics Research, Section B: Beam Interactions with Materials and Atoms 307 (2013) 536–540. doi:10.1016/j.nimb.2013.03.021.
[11] Q. Qi, G. Cheng, L. Shi, D. O'Connor, B. King, E. Kisi, Damage accumulation and recovery in C+-irradiated Ti3SiC2, Acta Materialia 66 (2014) 317–325. doi:10.1016/j.actamat.2013.11.019.
[12] M. K. Patel, D. J. Tallman, J. A. Valdez, J. Aguiar, O. Anderoglu, M. Tang, J. Griggs, E. Fu, Y. Wang, M. W. Barsoum, Effect of helium irradiation on Ti3AlC2 at 500C, Scripta Materialia 77 (2014) 1–4. doi:10.1016/j.scriptamat.2013.12.010.
[13] D. J. Tallman, E. N. Hoffman, E. N. Caspi, B. L. Garcia-Diaz, G. Kohse, R. L. Sindelar, M. W. Barsoum, Effect of neutron irradiation on select MAX phases, Acta Materialia 85 (2015) 132–143. doi:10.1016/j.actamat.2014.10.068.
[14] W. Jiang, C. H. Henager, T. Varga, H. J. Jung, N. R. Overman, C. Zhang, J. Gou, Diffusion of Ag, Au and Cs implants in MAX phase Ti3SiC2, Journal of Nuclear Materials 462 (2015) 310–320. doi:10.1016/j.jnucmat.2015.04.002.
[15] D. Clark, S. Zinkle, M. Patel, C. Parish, High temperature ion irradiation effects in MAX phase ceramics, Acta Materialia 105 (2016) 130–146. doi:10.1016/j.actamat.2015.11.055.
[16] J. Ward, S. Middleburgh, P. Frankel, M. Topping, A. Garner, D. Stewart, M. W. Barsoum, M. Preuss, Crystallographic evolution of MAX phases in proton irradiating environments, Journal of Nuclear Materials 502 (2018) 220–227. doi:10.1016/j.jnucmat.2018.02.008.
[17] M. Radovic, M. Barsoum, T. El-Raghy, S. Wiederhorn, W. Luecke, Effect of temperature, strain rate and grain size on the mechanical response of Ti3SiC2 in tension, Acta Materialia 50 (6) (2002) 1297–1306. doi:10.1016/S1359-6454(01)00424-4.
[18] A. Heinzel, A. Weisenburger, G. Müller, Long-term corrosion tests of Ti3SiC2 and Ti2AlC in oxygen containing LBE at temperatures up to 700C, Journal of Nuclear Materials 482 (2016) 114–123. doi:10.1016/j.jnucmat.2016.10.007.
[19] E. Hoffman, D. Vinson, R. Sindelar, D. Tallman, G. Kohse, M. Barsoum, MAX phase carbides and nitrides: Properties for future nuclear power plant in-core applications and neutron transmutation analysis, Nuclear Engineering and Design 244 (2012) 17–24. doi:10.1016/j.nucengdes.2011.12.009.
[20] D. J. Tallman, L. He, B. L. Garcia-Diaz, E. N. Hoffman, G. Kohse, R. L. Sindelar, M. W. Barsoum, Effect of neutron irradiation on defect evolution in Ti3SiC2 and Ti2AlC, Journal of Nuclear Materials 468 (2016) 194–206. doi:10.1016/j.jnucmat.2015.10.030.
[21] J. C. Nappé, C. Maurice, P. Grosseau, F. Audubert, L. Thomé, B. Guilhot, M. Beauvy, M. Benabdesselam, Microstructural changes induced by low energy heavy ion irradiation in titanium silicon carbide, Journal of the European Ceramic Society 31 (8) (2011) 1503–1511. doi:http://dx.doi.org/10.1016/j.jeurceramsoc.2011.01.002.
[22] D. J. Tallman, L. He, J. Gan, E. N. Caspi, E. N. Hoffman, M. W. Barsoum, Effects of neutron irradiation of Ti3SiC2 and Ti3AlC2 in the 121 − 1085C temperature range, Journal of Nuclear Materials 484 (2016) 120–134. doi:10.1016/j.jnucmat.2016.11.016.
[23] H. Zhang, J. Wang, J. Wang, Y. Zhou, S. Peng, X. Long, Role of Nanolaminated Crystal Structure on the Radiation Damage Tolerance of Ti3SiC2 : Theoretical Investigation of Native Point Defects, Journal of Nanomaterials 2013 (2013) 1–5. doi:10.1155/2013/831590.
[24] Q. Huang, R. Liu, G. Lei, H. Huang, J. Li, S. He, D. Li, L. Yan, J. Zhou, Irradiation resistance of MAX phases Ti3SiC2 and Ti3AlC2: Characterization and comparison, Journal of Nuclear Materials 465 (2015) 640–647. doi:10.1016/j.jnucmat.2015.06.056.
[25] W. K. Chu, Energy Loss of Charged Particles, in: J. P. Thomas, A. Cachard (Eds.), Material Characterization Using Ion Beams, Springer US, Boston, MA, 1978, pp. 3–34. doi:10.1007/978-1-4684-0856-0_1.
[26] S. J. Zinkle, L. L. Snead, Opportunities and limitations for ion beams in radiation effects studies : Bridging critical gaps between charged particle and neutron irradiations, Scripta Materialia 143 (2018) 154–160. doi:10.1016/j.scriptamat.2017.06.041.
[27] W. J. Weber, D. M. Duffy, L. Thomé, Y. Zhang, The role of electronic energy loss in ion beam modification of materials, Current Opinion in Solid State and Materials Science 19 (1) (2015) 1–11. doi:10.1016/j.cossms.2014.09.003.
[28] E. Zarkadoula, M. Toulemonde, W. J. Weber, Additive effects of electronic and nuclear energy losses in irradiation-induced amorphization of zircon, Applied Physics Letters 107 (26) (2015) 1–5. doi:10.1063/1.4939110.
[29] J. Nappé, I. Monnet, F. Audubert, P. Grosseau, M. Beauvy, M. Benabdesselam, Formation of nanosized hills on Ti3SiC2 oxide layer irradiated with swift heavy ions, Nuclear Instruments and Methods in Physics Research Section B: Beam Interactions with Materials and Atoms 270 (2012) 36–43. doi:10.1016/j.nimb.2011.09.027.
[30] H. Xue, E. Zarkadoula, R. Sachan, Y. Zhang, C. Trautmann, W. J. Weber, Synergistically-enhanced ion track formation in pre-damaged strontium titanate by energetic heavy ions, Acta Materialia 150 (2018) 351–359. doi:10.1016/j.actamat.2018.03.027.
[31] P. Eklund, M. Beckers, U. Jansson, H. Högberg, L. Hultman, The Mn+1AXn phases: Materials science and thin-film processing, Thin Solid Films 518 (8) (2010) 1851–1878. doi:10.1016/j.tsf.2009.07.184.
[32] Y. Zhang, M. L. Crespillo, H. Xue, K. Jin, C. H. Chen, C. L. Fontana, J. T. Graham, W. J. Weber, New ion beam materials laboratory for materials modification and irradiation effects research, Nuclear Instruments and Methods in Physics Research, Section B: Beam Interactions with Materials and Atoms 338 (2014) 19–30. doi:10.1016/j.nimb.2014.07.028.
[33] B. Liu, B. Petersen, Y. Zhang, J. Wang, W. J. Weber, Layered Structure Induced Anisotropic Low-Energy Recoils in Ti3SiC2, Journal of the American Ceramic Society 99 (8) (2016) 2693–2698. doi:10.1111/jace.14277.
[34] J. F. Ziegler, M. Ziegler, J. Biersack, SRIM The stopping and range of ions in matter (2010), Nuclear Instruments and Methods in Physics Research Section B: Beam Interactions with Materials and Atoms 268 (11-12) (2010) 1818–1823. doi:10.1016/j.nimb.2010.02.091.
[35] J. F. Ziegler, J. P. Biersack, M. D. Ziegler, SRIM 2013, Software code. SRIM - The Stopping and Range of Ions in Matter (2013).
[36] M. Crespillo, J. Graham, Y. Zhang, W. Weber, Temperature measurements during high flux ion beam irradiations, Review of Scientific Instruments 87 (2) (2016) 1–7. doi:10.1063/1.4941720.
[37] B. Henke, E. Gullikson, J. Davis, X-ray interactions: photoabsorption, scattering, transmission, and reflection at e=50-30000 ev, z=1-92, Atomic Data and Nuclear Data Tables 54 (no.2) (1993) 181–342.
[38] M. Marciszko, Diffraction study of mechanical properties and residual stresses resulting from surface processing of polycrystalline materials, AGH - University of Science and Technology, 2013.
[39] H. M. Rietveld, A profile refinement method for nuclear and magnetic structures, Journal of Applied Crystallography 2 (2) (1969) 65–71.

doi:10.1107/S0021889869006558.
[40] A. C. Larson, R. B. Von Dreele, General Structure Analysis System (GSAS), Structure 748 (LAUR 86-748) (2004) 86–748. arXiv:0805.4630, doi:10.1103/PhysRevLett.101.107006.
[41] OriginPro (OriginLab, Northampton, MA).
[42] M. Marciszko, A. Baczmański, M. Wróbel, W. Seiler, C. Braham, S. Wroński, R. Wawszczak, Problem of elastic anisotropy and stacking faults in stress analysis using multireflection grazing-incidence X-ray diffraction, Journal of Applied Crystallography 48 (2015) 492–509. doi:10.1107/S1600576715002666.
[43] M. Marciszko, A. Baczmański, C. Braham, M. Wróbel, W. Seiler, S. Wroński, K. Berent, Analysis of stresses and crystal structure in the surface layer of hexagonal polycrystalline materials: A new methodology based on grazing incidence diffraction, Journal of Applied Crystallography 49 (2016) 85–102. doi:10.1107/S1600576715021810.
[44] V. Hauk, Structural and Residual Stress Analysis by Nondestructive Methods, Elsevier Science B.V., Amsterdam, 1997.
[45] A. Baczmanski, C. Braham, W. Seiler, N. Shiraki, Multi-reflection method and grazing incidence geometry used for stress measurement by X-ray diffraction, Surface and Coatings Technology 182 (1) (2004) 43–54. doi:10.1016/j.surfcoat.2003.07.005.
[46] T. Yang, C. Wang, W. Liu, S. Liu, J. Xiao, Q. Huang, J. Xue, S. Yan, Y. Wang, Formation of nano-twinned structure in Ti3AlC2 induced by ion-irradiation, Acta Materialia 128 (2017) 1–11. doi:10.1016/j.actamat.2017.01.066.
[47] J. Xiao, T. Yang, C. Wang, J. Xue, Y. Wang, Investigations on radiation tolerance of Mn+1AXn phases: Study of Ti3SiC2, Ti3AlC2, Cr2AlC, Cr2GeC, Ti2AlC, and Ti2AlN, Journal of the American Ceramic Society 98 (4) (2015) 1323–1331. doi:10.1111/jace.13450.
[48] S. C. Middleburgh, G. R. Lumpkin, D. Riley, Accommodation, accumulation, and migration of defects in Ti3 SiC2 and Ti3 AlC2 MAX phases, Journal of the American Ceramic Society 96 (10) (2013) 3196–3201. doi:10.1111/jace.12537.
[49] L. Thomé, G. Velisa, S. Miro, A. Debelle, F. Garrido, G. Sattonnay, S. Mylonas, P. Trocellier, Y. Serruys, Recovery effects due to the interaction between nuclear and electronic energy losses in SiC irradiated with a dual-ion beam, Journal of Applied Physics 117 (10) (2015) 1–9. doi:10.1063/1.4914305.
[50] H. Xue, Y. Zhang, W. J. Weber, In-cascade ionization effects on defect production in 3C silicon carbide, Article in Materials Research Letters 5 (7) (2017) 494–500. doi:10.1080/21663831.2017.1334241.
[51] P. Liu, Y. Zhang, H. Xue, K. Jin, M. L. Crespillo, X. Wang, W. J. Weber, A coupled effect of nuclear and electronic energy loss on ion irradiation damage in lithium niobate, Acta Materialia 105 (2016) 429–437. doi:10.1016/j.actamat.2015.12.048.
[52] N. Sellami, M. L. Crespillo, H. Xue, Y. Zhang, W. J. Weber, Role of atomic-level defects and electronic energy loss on amorphization in LiNbO3 single crystals, Journal of Physics D: Applied Physics 50 (32) (2017) 325103. doi:10.1088/1361-6463/aa7a9e.
[53] N. Sellami, M. L. Crespillo, Y. Zhang, W. J. Weber, Two-stage synergy of electronic energy loss with defects in LiTaO3 under ion irradiation irradiation, Materials Research Letters 6 (6) (2018) 399–344. doi:10.1080/21663831.2018.1455753.